Experimental Study of Slow Cyclotron Maser Operation in Weakly Relativistic Region

Kiyoshi BANSHO, Kazuo OGURA, Hiroaki OE, Yusuke KAZAHARI, Hiroshi IIZUKA, Akira SUGAWARA, Takashi SHIMOZUMA[1)], Sakuji KOBAYASHI[1)] and Kohji OKADA[1)]

Graduate School of Science and Technology, Niigata University, Niigata 950-2181, Japan
[1)]*National Institute for Fusion Science, 322-6 Oroshi-cho, Toki 509-5292, Japan*

(Received 8 January 2009 / Accepted 3 August 2009)

Studies of slow cyclotron maser operation of a slow-wave device are presented. The beam voltage is weakly relativistic, less than 100 kV. The slow-wave structure is a periodically corrugated oversized waveguide for K-band operation. When using rectangular corrugation having a relatively small ratio of corrugation width to periodic length of about 20 %, the dispersion curve near the upper cut-off becomes flat and second harmonic slow cyclotron maser operation is observed in the low-energy region near 30 kV. Another type of combined resonance of Cherenkov and slow cyclotron interaction is also demonstrated in which an absolute instability is driven by the slow cyclotron interaction. By using sinusoidal corrugation and rectangular corrugation having a 50 % ratio of corrugation width to periodic length, amplification effects due to the fundamental and second harmonic slow cyclotron interactions are observed.

© *2010 The Japan Society of Plasma Science and Nuclear Fusion Research*

Keywords: slow cyclotron maser, Cherenkov interaction, weakly relativistic beam, periodic corrugation, slow-wave device

DOI: 10.1585/pfr.5.S1049

1. Introduction

Backward wave oscillators (BWOs) are high-power microwave sources. In BWOs, slow wave structures (SWSs) are used to reduce the phase velocity of electromagnetic waves to beam velocity. An axially streaming electron beam interacts with the electromagnetic field to generate high-power microwaves. To increase the power handling capability and/or operating frequency, oversized SWSs have been used successfully. Here, "oversized" means that the diameter D of the SWS is larger than the free-space wavelength λ of the output electromagnetic wave by several times or more. Output powers up to tens of GW are obtained by using sinusoidally corrugated or smoothly curved SWSs [1, 2]. Smoothly curved corrugations are important to prevent discharges in the SWS due to strong electric fields. However, their fabrication and analysis become very difficult in the oversized case. For moderate power levels of MW or less, discharge in the SWS may not be a serious problem. To overcome the manufacturing and analytical difficulties of smoothly curved corrugation, a rectangularly corrugated SWS is often used as an alternative [3].

Although the radiation based on the Cherenkov interaction is predicted to be independent of the magnetic field strength, some strong magnetic field dependence of the output power can be seen in the cyclotron resonance region [3–8]. The output power may decrease or increase depending on experimental conditions. Power drops are attributed to fast cyclotron resonance absorption at the normal Doppler-shifted frequency. For power increase, one possible mechanism is the slow cyclotron interaction at the anomalous Doppler-shifted frequency [6–10]. In the slow cyclotron maser of Refs. [6,7], a backward wave generated by the Cherenkov interaction is amplified by forward wave interaction at the slow cyclotron resonance. Ref. [8] experimentally demonstrates that this kind of combined operation can also be realized by the second harmonic slow cyclotron interaction. In these oversized SWS operations, generation, amplification, and absorption of microwaves by the slow and fast cyclotron and Cherenkov interactions should be carefully controlled. The magnetic field dependence of slow-wave devices remains unclear. Moreover, the problem of mode control is still far from being fully elaborated.

In this study, we investigate how the operating characteristics of oversized slow-wave devices depend on the magnetic field in terms of the slow cyclotron interaction. We use two types of rectangularly corrugated SWSs. The upper cut-off frequency of the fundamental mode is about 25 GHz for both SWSs. One has dispersion characteristics parallel to those of the sinusoidal SWS, and the other has dispersion characteristics that can be newly realized by using rectangular corrugation [8]. Our beam source is a novel disk cathode [3]. It can generate a uniformly distributed annular beam in the weakly relativistic region. We examine the performance of a slow cyclotron maser in the weakly relativistic region using rectangularly and sinu-

author's e-mail: f08e078g@mail.cc.niigata-u.ac.jp

© 2010 The Japan Society of Plasma Science and Nuclear Fusion Research

soidally corrugated SWSs.

2. Slow Wave Structure (SWS)

The cylindrical SWS has a periodically corrugated wall. The corrugation is rectangular or sinusoidal. In Fig. 1, the rectangularly corrugated SWS is shown. Dispersion characteristics of an SWS are determined by the average radius R_0, corrugation amplitude h, and periodic length z_0. The radius R_0 is the center point between the top and bottom of the corrugations. The corrugation wave number is given by $k_0 = 2\pi/z_0$. The rectangular corrugation has one more parameter, the corrugation width d. The dispersion characteristics of a structure are controlled by changing R_0, h, d, and z_0.

Dispersion curves of the rectangularly corrugated SWS are obtained by a numerical method based on the mathematical formula in Ref. [11]. Figures 2 (a) and (b) show the dispersion relation of the fundamental axisymmetric transverse magnetic (TM_{01}) mode for two types. For oversized periodic SWSs, the fundamental nonaxisymmetric hybrid HE_{11} mode exists very close to the TM_{01} mode [12]. In this paper, dispersions like those in Figs. 2 (a) and (b) are called the A and B types, respectively. Their parameters are listed in Table 1. In Fig. 2, beam lines of the space charge mode, $\omega = k_z v$, and slow cyclotron mode, $\omega = k_z v - \Omega$, are also plotted. Here, ω, k_z, v, and Ω are the angular frequency, axial wave number, beam velocity, and relativistic cyclotron frequency, respectively. The slow space charge and slow cyclotron modes couple to the fundamental mode, leading to the Cherenkov and slow cyclotron instabilities.

For the A type, the Cherenkov instability of an 80 keV beam is absolute. In this case, the group velocity of TM_{01} is negative, and BWO operation by the Cherenkov mechanism is possible. The beam interaction point with TM_{01} is close to the upper cut-off at the π-point. Above about 90 kV, BWO operation by the Cherenkov interaction becomes impossible because the group velocity of TM_{01} becomes positive at the intersection point. For the B type, the dispersion curve around the upper cut-off becomes very flat. Above 60 keV, the intersection of the space charge

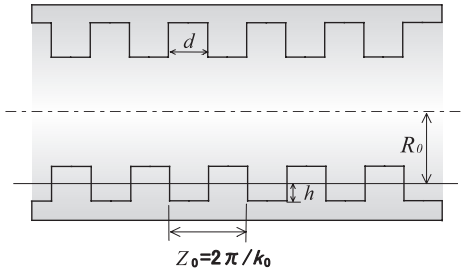

Fig. 1 Periodically corrugated cylindrical SWS.

Table 1 Parameters of rectangularly corrugated SWS

	R_0 [mm]	h [mm]	z_0 [mm]	d/z_0 [%]
A	15.1	1.1	3	50
B	15.38	1.38	2.2	22.7

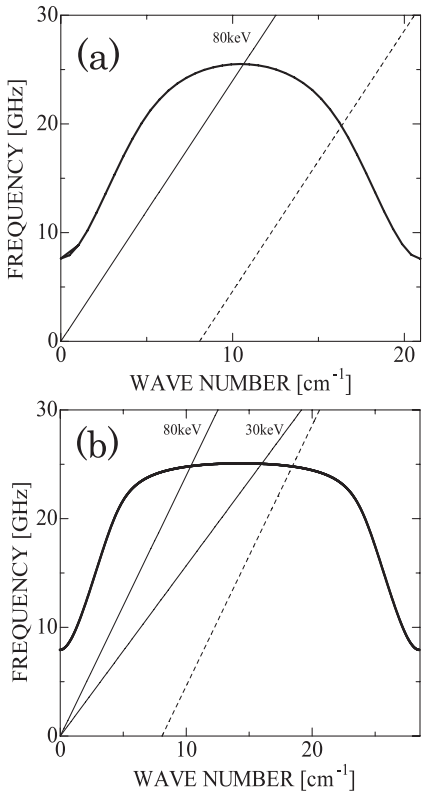

Fig. 2 Dispersion characteristics of TM_{01} for rectangularly corrugated SWS, (a) A type and (b) B type. Solid and dashed lines represent slow space charge and slow cyclotron modes, respectively at 0.8 T.

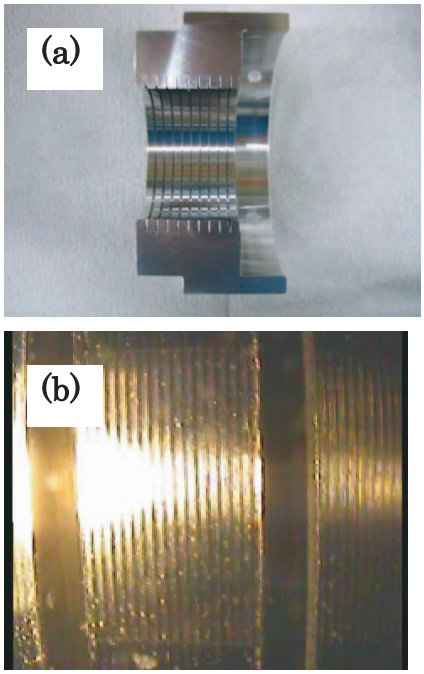

Fig. 3 Rectangular corrugation of B-type SWS.

mode and TM_{01} shifts to a traveling wave region. Hence, BWO operation by the Cherenkov interaction becomes impossible. With a decrease in beam energy to 30 keV, the interaction point moves to a backward wave region as shown in Fig. 2 (b). If the slow cyclotron interaction is considered, an absolute instability can occur in the backward wave region even for 80 kV as shown in Fig. 2 (b).

Dispersion curves like those in Fig. 2 (a) can also be realized by sinusoidal corrugations. However, the flat pattern in Fig. 2 (b) requires a relatively small value of d/z_0 and cannot be realized by sinusoidal corrugations. A cross section of B-type corrugation is shown in Fig. 3 (a); an enlargement of a small area appears in Fig. 3 (b). Fine lines in Fig. 3 (b) are grinding marks of the lathe cutting tool. The arithmetic mean roughness and the maximum height of roughness are about 1.6 μm and 6.3 μm, respectively. And it can be said the surface is smooth enough for K-band operation.

3. Experimental Results

The experimental setup is schematically shown in Fig. 4. An output voltage up to 100 kV from the pulse-forming line is applied to a cold cathode. The disk cathode proposed in Ref. [3] is used as the cold cathode. A uniform axial magnetic field B_0 for beam propagation is provided by 10 solenoid coils. The value of B_0 can be changed from 0 to about 1 T. The microwave output is picked up by a rectangular horn antenna typically located 600 mm from the output window.

Figure 5 shows an example of detected signals with an A-type SWS. The beam voltage and current are about 100 kV and 300 A, respectively at the time of the microwave peak. The microwave signal is split into two branches. One consists of a short waveguide and forms a prompt signal. The other is a delay line and forms a delayed signal. The operation frequency estimated from the delay time is about 26 GHz.

In Ref. [12], the oscillation starting condition is studied for an oversized BWO composed of a sinusoidally corrugated oversized SWS. A critical beam voltage (starting voltage) and current (starting current) for the meaningful radiation exist. The starting current is expected to be about 10 A or less, which is easily cleared by the cold cathode. The starting voltage is more stringent than the starting current for an oversized BWO [12]. This is true for oversized BWOs with both A- and B-type rectangular corrugations. Figure 5 corresponds to oversized BWO operation by the Cherenkov interaction above the starting voltage.

Figure 6 is an example of the waveform of measured

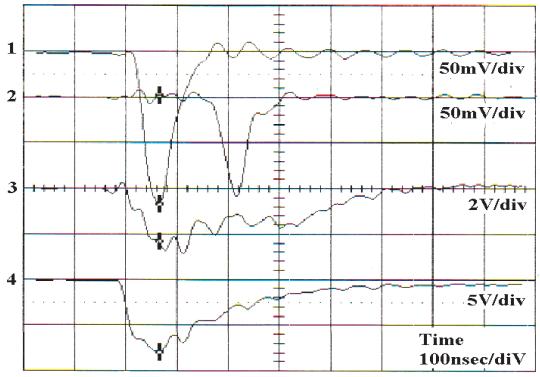

Fig. 5 Waveform of measured signals for A type: 1, prompt signal; 2, delayed signal; 3, beam current; and 4, beam voltage.

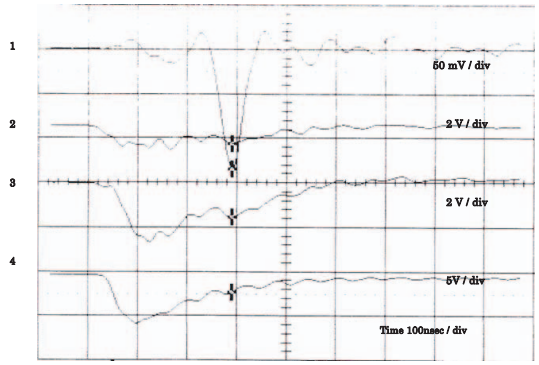

Fig. 6 Waveform of measured signals for B type: 1, microwave output; 2, cathode current; 3, beam current; and 4, beam voltage.

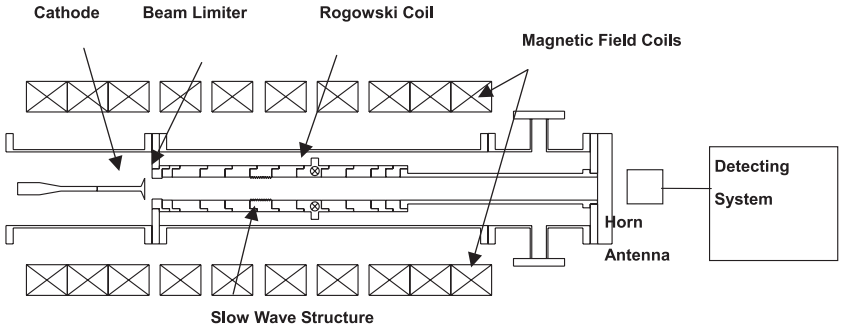

Fig. 4 Schematic diagram of the experimental setup.

signals for a B-type SWS. The applied beam voltage is about 80 kV. However, no radiation occurs until the voltage decreases to about 30 kV. As explained in the previous section, the space charge mode intersects the fundamental slow wave in the travelling wave region above about 60 keV, and BWO operation due to the Cherenkov interaction will not start. For about 30 kV, the interaction point is in a backward wave region. However, the starting condition of BWO is not fulfilled. Hence, another oscillation mechanism than the Cherenkov one is required for the radiation of Fig. 6. Figure 7 shows the power dependence on B_0 for a B-type SWS with about 30 kV. The radiation resonantly increases around 0.6 T. This is the slow cyclotron maser operation reported in Ref. [8]. In this operation, the oscillation of the absolute instability due to the Cherenkov interaction is resonantly amplified by the second harmonic slow cyclotron interaction, as is discussed based on numerical analysis in the next section.

Because it is difficult to fabricate a B-type SWS, rectangular disks corresponding to each rectangular corrugation part are made separately in Ref. [8] and then put together into one SWS section. For such disk-integrated SWS, the homogeneity among corrugations is hard to evaluate and may be inferior. In this work, one SWS section is manufactured as one piece, as shown in Fig. 3. Its manufacturing accuracy is on the order of 0.01 mm. The power level of Fig. 7 is about three times that of the disk-integrated SWS of Ref. [8].

By changing the SWS end conditions, the radiation mode can be controlled, as reported in Refs. [3, 8]. For Fig. 7, a straight cylinder 68 mm long is placed at the beam entrance of the SWS. The radiation patterns show that the radiation of Fig. 7 is the HE_{11} mode. By changing the cylinder length to 34 mm, the radiation mode changes to the TM_{01} mode. The power dependence on B_0 is depicted in Fig. 8 (a). The effect of the slow cyclotron interaction is observed above 0.6 T. However, the output decreases around 0.7 T. This might be caused by the effect of absorption due to the fast cyclotron interaction in the straight cylinder before and after the SWS, as discussed below. In Fig. 7, the absorption might also occur, but is not so conspicuous.

As mentioned in the previous section, BWO operation due to the Cherenkov interaction is not expected above 60 kV for a B-type SWS (Fig. 2). However, the slow cyclotron interaction can exist in the backward wave region and causes an absolute instability even above 60 kV, as in Fig. 2 (b). In this case, the oscillation due to the slow cyclotron interaction is amplified by the Cherenkov interaction. The corresponding radiation is observed experimentally by increasing the beam current as well as the beam voltage. Beam current is controlled by the gap between cathode and anode. The radiation is observed at current and voltage values of about 500 A and 75 kV, respectively, and the power dependence on B_0 is shown in Fig. 8 (b). The output decreases around 0.7 T due to the fast cyclotron absorption, as in Fig. 8 (a). Although Figs. 8 (a) and (b) show a similar pattern, they result from completely different combined resonances. The critical beam current for the combined resonance of Fig. 8 (b) is much higher than for that of Fig. 8 (a). Some modified versions of a B-type SWS are tested with $h = 1.38$ mm and 1.31 mm and $d/z_0 = 22.7\,\%$ and 20 %. The essential features of radiation remain the same in the modified SWSs.

The effect of slow cyclotron resonance is also observed for an A-type SWS with a relatively low beam voltage of less than 50 kV, as shown in Fig. 9 (a). The microwave output increases around 0.5 T and 0.9 T. Slow cyclotron interactions are expected to occur at 0.98 T for the

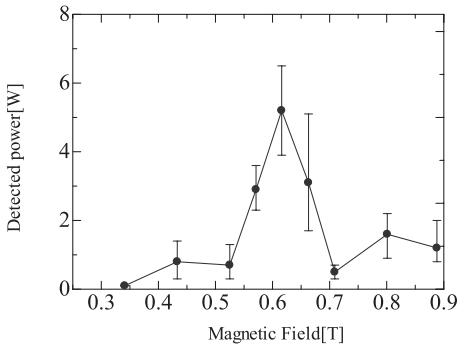

Fig. 7 Output power versus magnetic field for a 10-period B-type SWS. Beam voltage and current are about 30 kV and 150 A, respectively.

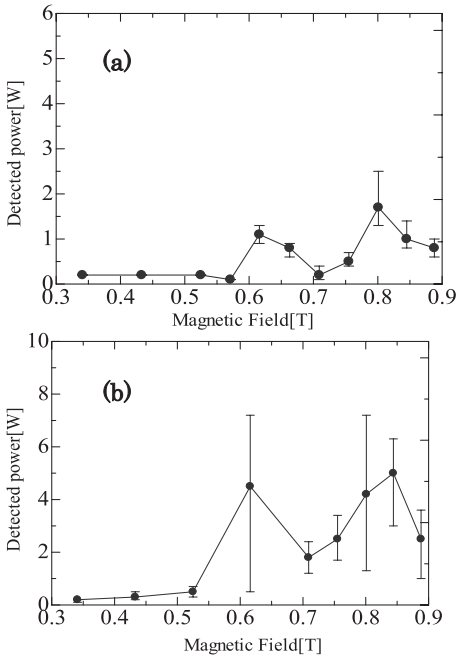

Fig. 8 Output power versus magnetic field for a 10-period B-type SWS. Beam voltage and current are (a) about 30 kV and 130 A and (b) about 75 kV and 500 A, respectively.

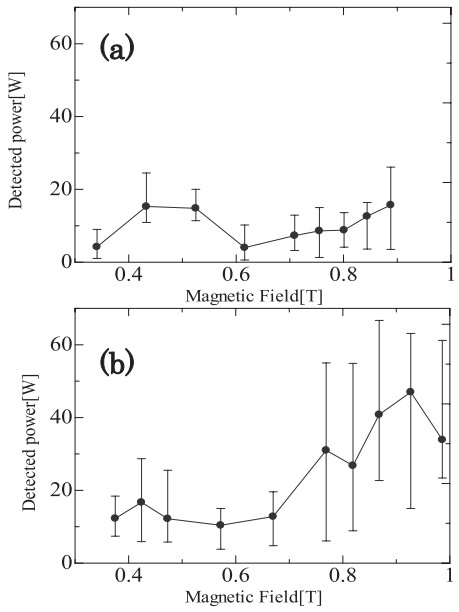

Fig. 9 Output power versus magnetic field for (a) 20-period rectangularly corrugated A-type SWS and (b) 50-period sinusoidally corrugated SWS. Beam voltage and current are (a) about 35 kV and 100 A, and (b) about 40 kV and 150 A.

A type and 1.35 T for the B type. The expected resonant magnetic field for the A type is lower than that for the B type. The dispersion characteristics of A type are realized by sinusoidal corrugations; a similar amplification effect due to slow cyclotron resonance is expected at 0.84 T and is experimentally observed, as shown in Fig. 9 (b). Power increases can be seen, more clearly than in Fig. 9 (a), at about 0.9 T and 0.45 T, corresponding to the slow cyclotron interaction at the fundamental and second harmonics, respectively.

4. Discussion and Conclusion

For a B-type SWS, the dispersion relation of the TM_{01} mode is shown in Fig. 10, including the beam effects using the field theory in Ref. [13] based on an infinitesimally thin annular beam. According to Floquet's theorem (known as Bloch's theorem in solid-state physics), the dispersion curves of a spatially periodic SWS are periodic in wave number space. For a spatially periodic SWS with a period of z_0, the corresponding period in k_z-space is $k_0 = 2\pi/z_0$. Since a one-period drawing has all the information we need, the dispersion relation is depicted about one period of $0 < k_z < k_0$ in Fig. 10 with $k_0 = 28.5\,\mathrm{cm}^{-1}$. Other regions of k_z-space are reduced to the region of $0 < k_z < k_0$. For example, the forward region of the TM_{01} mode from $28.5\,\mathrm{cm}^{-1}$ ($k_z z_0 = 2\pi$) to $42.8\,\mathrm{cm}^{-1}$ ($k_z z_0 = 3\pi/2$) can be seen in the forward region from 0 ($k_z z_0 = 0$) to $14.3\,\mathrm{cm}^{-1}$ ($k_z z_0 = \pi/2$).

In Fig. 10, oscillation occurs at the Cherenkov interaction point because it is an absolute instability. The slow

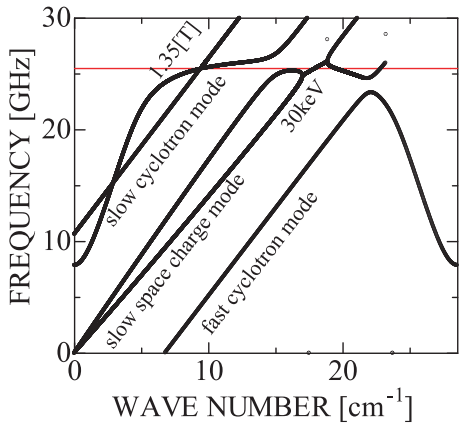

Fig. 10 Dispersion curves of fundamental TM_{01} mode for B-type SWS. Beam energy and current are 30 keV and 200 A, respectively.

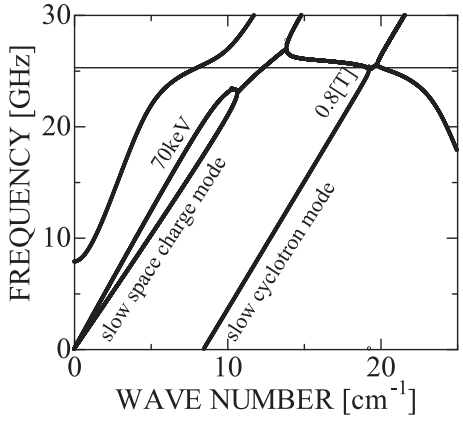

Fig. 11 Dispersion curves of fundamental TM_{01} Mode for B-type SWS. Beam energy and current are 70 keV and 800 A, respectively.

cyclotron mode depends on the axial magnetic field B_0. With increasing B_0, the slow cyclotron mode $\omega = k_z v - \Omega$ shifts to the right in Fig. 10. With a further increase in B_0, the slow cyclotron mode leaves the region of $0 < k_z < k_0$, and the periodic line in $-k_0 < k_z < 0$ comes from the left of Fig. 10. The Cherenkov oscillation synchronizes resonantly with the slow cyclotron amplification at about 1.35 T. This is the slow cyclotron maser operation reported in Refs. [6–10]. The hybrid HE_{11} mode exists very close to the TM_{01} mode and the corresponding resonance magnetic is almost the same. The radiation of Fig. 7 corresponds to this combined resonance at the second harmonic slow cyclotron interaction. By using A-type and sinusoidally corrugated SWSs, the magnetic field of the combined resonance decreases. Amplification effects corresponding to the second and fundamental slow cyclotron interactions are observed.

For a B type SWS, another kind of combined resonance can occur, as shown in Fig. 11. In this case, absolute instability is driven by the slow cyclotron interaction. Mi-

crowaves are generated by the slow cyclotron absolute instability and amplified by the Cherenkov interaction. This combined resonance is different from that in Fig. 10. To realize this kind of resonance in the weakly relativistic region, a very flat upper cut-off is required. Figure 8 (b) is the first experimental demonstration of this combined resonance. The critical beam current is about 500 A in our case.

It is true that an absolute instability at the saddle point can spontaneously generate signals because of the natural feedback mechanism of the backward wave. This feedback mechanism is effective regardless of the end reflections. However, it has been shown experimentally that the oscillations depend on the end conditions of the SWS [3, 8]. Thus, the experimentally observed oscillations might not be caused by the natural feedback mechanism. In a finite-length SWS, the reflections at both ends impose an axial boundary condition and provide an additional feedback mechanism [12]. The starting current and voltage come from the imaginary and real parts, respectively, of the axial condition. The real part means that the width of the unstable region in wave number space should be on the order of $2\pi/L$ for an SWS of length L. For oscillations to start, the presence of an absolute instability is a sufficient condition [14]. If the unstable region around the absolute instability is wide enough, oscillation can start. In the oversized BWO operation shown in Fig. 5, the absolute instability with sufficient unstable width is driven by the Cherenkov interaction. In slow cyclotron maser operation, the slow cyclotron interaction is added to the feedback mechanism. In this paper, two types of feedback mechanisms are demonstrated. In the first, the Cherenkov interaction drives the absolute instability, and the slow cyclotron interaction drives convective instability. In the second, the roles of Cherenkov and slow cyclotron interactions are just the opposite. Convective instability may oscillate signals if an adequate feedback mechanism exists. However, so far oscillations due only to, convective instability have not been observed in our experiments with the oversized SWS.

Based on numerically obtained growth rates and interaction widths of the Cherenkov and slow cyclotron instabilities, the radiation oscillation peak is expected to be about 0.65 T with an oscillation area of about 0.6 T to 0.8 T for Figs. 7 and 8 (a). The oscillation area becomes rather broad due to the flat upper cut-off. For Fig. 8 (b), the expected oscillation peak is around 0.7 T with an oscillation area of about 0.45-0.9 T. In Figs. 8 (a) and (b), the microwave power decreases around 0.7 T. The corresponding absorption can be seen in Fig. 7, although the dip is indistinct. One possible mechanism for these power drops is absorption by the fast cyclotron interaction. The absorption may occur in the SWS and in the drift section consisting of a straight waveguide before and after the SWS. With increasing B_0, the fast cyclotron mode $\omega = k_z v + \Omega$ moves in the opposite direction to the slow cyclotron mode. For the TM_{01} mode in a B-type SWS show in Figs. 10 and 11, resonant absorption is expected to occur below 0.5 T, and it is expected to occur around 0.6-0.7 T in the drift section. The power dips of Figs. 7 and 8 might be attributed to the absorption effect in the drift section. Qualitatively, the radiation regions in Figs. 7 and 8 agree fairly well with the numerically expected regions. For a more definitive study of slow cyclotron maser operation, including power dips, it is necessary to control the absorption as well as the oscillation and amplification. It is also important to analyze the effect of end reflections on the slow cyclotron maser.

In conclusion, we studied the performance of a slow cyclotron maser in the weakly relativistic region using rectangularly and sinusoidally corrugated SWSs. The SWS is an oversized waveguide for K-band operation. By using rectangular corrugation with a relatively small ratio of corrugation width to periodic length of about 20 %, a very flat upper cut-off is realized. In the low-energy region near 30 kV, the Cherenkov instability becomes absolute, and maser operation of second harmonic slow cyclotron interaction is observed. Moreover, another type of combined resonance is demonstrated for the first time, in which the absolute instability is the slow cyclotron one. The Cherenkov interaction amplifies the signal. By using sinusoidal and rectangular corrugations having corrugation width to periodic length ratio of 50 %, the amplification effect of the slow cyclotron interaction at both the fundamental and second harmonics are observed.

Acknowledgments

This work was performed partly under the collaboration organized by NIFS (NIFS08KCRR006 and NIFS07KUGM026) and partially supported by a Grant-in-Aid for Scientific Research from the Japan Society for the Promotion of Science.

[1] S. P. Bugaev *et al.*, IEEE Trans. Plasma Sci. **18**, 518 (1990).
[2] S. P. Bugaev *et al.*, IEEE Trans. Plasma Sci. **18**, 525 (1990).
[3] K. Ogura *et al.*, IEEJ Trans. FM **127**, 681 (2007).
[4] Yu. V. Tkach *et al.*, Fiz. Plasmy **5**, 1021 (1979).
[5] Y. Carmel *et al.*, Phys. Fluids **B4**, 2286 (1992).
[6] Md. R. Amin *et al.*, J. Phys. Soc. Jpn. **67**, 4473 (1995).
[7] K. Ogura *et al.*, Phys. Rev. E **53**, 2726 (1996).
[8] Y. Takamura *et al.*, Plasma Fusion Res. **3**, S1078 (2008).
[9] K. Ogura *et al.*, J. Phys. Soc. Jpn. **67**, 3462 (1998).
[10] K. Ogura *et al.*, Trans. Fusion Tech. **39**, 320 (2001).
[11] P. J. Clarricoats and A. D Olver, *Corrugated Horns for Microwave Antenna* (Peter Peregrinus, London, 1984).
[12] K. Ogura *et al.*, J. Plasma Fusion Res. SERIES **6**, 703 (2004).
[13] K. Ogura *et al.*, J. Plasma Phys. **72**, 905 (2006).
[14] E. M. Lifshitz and L. P. Pitaevskii, *Physical Kinetics* (Pergamon, New York, 1981) Chapter VI.